

# Robustness of spin-coupling distributions for perfect quantum state transfer

Analia Zwick,<sup>1,2,\*</sup> Gonzalo A. Álvarez,<sup>1,†</sup> Joachim Stolze,<sup>1,‡</sup> and Omar Osenda<sup>2,§</sup>

<sup>1</sup>*Fakultät Physik, Technische Universität Dortmund, D-44221 Dortmund, Germany.*

<sup>2</sup>*Facultad de Matemática, Astronomía y Física and Instituto de Física Enrique Gaviola, Universidad Nacional de Córdoba, 5000 Córdoba, Argentina.*

The transmission of quantum information between different parts of a quantum computer is of fundamental importance. Spin chains have been proposed as quantum channels for transferring information. Different configurations for the spin couplings were proposed in order to optimize the transfer. As imperfections in the creation of these specific spin-coupling distributions can never be completely avoided, it is important to find out which systems are optimally suited for information transfer by assessing their robustness against imperfections or disturbances. We analyze different spin coupling distributions of spin chain channels designed for perfect quantum state transfer. In particular, we study the transfer of an initial state from one end of the chain to the other end. We quantify the robustness of different coupling distributions against perturbations and we relate it to the properties of the energy eigenstates and eigenvalues. We find that the localization properties of the systems play an important role for robust quantum state transfer.

PACS numbers: 03.67.Hk, 03.65.Yz, 75.10.Pq, 75.40.Gb

## I. INTRODUCTION

Quantum information processing has been extensively studied during the past years [1]. One of the main challenges of actual physical implementations has been the manipulation of the quantum information with sufficient accuracy to prevent errors. In particular it is important to be able to transfer quantum information between different elements of a quantum computer [2]. In this respect, spin chain systems have been proposed as quantum channels for the transmission of quantum states, where the spins act as the quantum bits [3–10]. Many systems of this kind have been explored in order to improve their performance for the state transmission. One of the goals is to find systems that allow for state transfer without any dynamical manipulations during the transfer procedure or with only minimal additional requirements. For example, local control only on the boundary spins in either an initialized chain [11, 12] or an unpolarized chain [13, 14] can cause a large enhancement of the transmission fidelity from one end of the chain to the opposite end; even perfect state transfer (PST) could be achieved by engineering the entire set of spin-spin couplings in the chain [15–18].

Very few of these systems have been implemented experimentally, for example using small numbers of spins in liquid state NMR [19–23] and slightly larger numbers of them in solid-state NMR [24, 25]. Spin defects in diamond seem to show a promising direction for near future implementations [26–28]. Important experimental challenges are posed by the lack of individual addressability

of the spins and, more importantly, by their vulnerability to decoherence [29]. Imperfections in the implementation of spin-chain systems also cause decoherence and were predicted to produce localization of the quantum information [30–33] which was recently demonstrated experimentally [34]. Consequently, a successful characterization of these PST protocols should consider these errors in order to find the optimal one. Two PST protocols that require engineered spin-couplings [16, 17] have been analyzed in this respect considering static perturbations [18, 30, 35]. Other important points to consider are the timing errors on the time when the PST is achieved [18] and the speed of transfer of the different protocols [36]. But, considering that the number of possible systems that could be used for PST [17, 18] is infinite, a performance comparison between them should be aimed at finding a system which is as robust against perturbations as possible. For that purpose it is important to find out which intrinsic properties of a system make it robust against perturbations. In this work, we tackle these questions analyzing different energy distributions that allow for PST and compare their robustness against static perturbations. We characterize the robustness of the systems by calculating their transmission fidelity. In order to find the relevant properties of the systems that make them robust, we analyze how the eigenstates and eigenenergies are perturbed. We find that the localization properties of a system are intimately connected to its robustness.

The paper is organized as follows, in Sec. II we present the XX model describing the quantum spin chain and the necessary conditions for perfect state transfer. In Sec. III we analyze different energy eigenvalue configurations of the system and the corresponding spin-coupling distributions. In Sec. IV A we analyze the fidelity of the transfer of the different configurations, and the influence of perturbations on the transmission is discussed in Section IV B. Subsequently, in Sec. V, we analyse how the indi-

---

\*Electronic address: [zwick@famaf.unc.edu.ar](mailto:zwick@famaf.unc.edu.ar)

†Electronic address: [galvarez@e3.physik.uni-dortmund.de](mailto:galvarez@e3.physik.uni-dortmund.de)

‡Electronic address: [joachim.stolze@tu-dortmund.de](mailto:joachim.stolze@tu-dortmund.de)

§Electronic address: [osenda@famaf.unc.edu.ar](mailto:osenda@famaf.unc.edu.ar)

vidual perturbed eigenstates and eigenvalues contribute to the dynamics of quantum information transport. Finally, in Sec. VI we give the conclusions.

## II. PERFECT STATE TRANSFER CHANNELS

We consider a chain of  $N$  spins 1/2 (qubits) with a modulated XX interaction between nearest neighbors. Taking into account an external magnetic field, the Hamiltonian is

$$H = \sum_i \frac{J_i}{2} (\sigma_i^x \sigma_{i+1}^x + \sigma_i^y \sigma_{i+1}^y) - \sum_i \frac{b_i}{2} \sigma_i^z, \quad (1)$$

where  $\sigma_i^u$  are the Pauli operators of the  $i$ th spin,  $b_i$  is the local external field and  $J_i$  is the exchange coupling.

The aim is to transmit a quantum state  $|\psi_0\rangle$  stored on the first spin ( $i = 1$ ) to the last spin of the chain ( $i = N$ ), where  $|\psi_0\rangle = \alpha|0\rangle + \beta|1\rangle$  is a given superposition of a spin down and up respectively and the remaining spins of the chain are initialized in the spin down state. The Hamiltonian (1) preserves the total magnetization along the  $z$ -axis because  $[H, \sum_i \sigma_i^z] = 0$ , *i.e.*, the number of excited spins is conserved. Because the initial state  $|\Psi_0\rangle$  is a superposition of the eigenstate  $|\mathbf{0}\rangle = |0\dots 0\rangle$  and the state  $|\mathbf{1}\rangle = |1_1 0\dots 0\rangle$ , the component  $|\mathbf{0}\rangle$  is conserved and the component  $|\mathbf{1}\rangle$  evolves within the one excitation subspace spanned by the basis states  $|\mathbf{i}\rangle = |0\dots 0 1_i 0\dots 0\rangle$ . The state of the system at a given evolution time  $t$  is

$$|\Psi(t)\rangle = e^{-iHt/\hbar} |\Psi_0\rangle = \alpha|\mathbf{0}\rangle + \beta \sum_{i=1}^N f_i(t) |\mathbf{i}\rangle, \quad (2)$$

where  $f_i(t) = \langle \mathbf{i} | e^{-iHt/\hbar} | \mathbf{1} \rangle$ . To measure the effectiveness of state transfer between sites 1 and  $N$ , we determine the fidelity  $\mathcal{F}(t) = \langle \Psi_0 | \rho_N(t) | \Psi_0 \rangle$  averaged over all possible initial states  $|\Psi_0\rangle$  distributed uniformly over the Bloch sphere, which is given by [3]

$$F(t) = \frac{|f_N(t)| \cos \gamma}{3} + \frac{|f_N(t)|^2}{6} + \frac{1}{2}, \quad (3)$$

where  $\gamma = \arg |f_N(t)|$ . Because the phase  $\gamma$  can be controlled by an external field once the state is transferred, we consider  $\cos \gamma = 1$ . PST is achieved when  $F = 1$ .

For a spin chain possessing mirror symmetry with respect to the center, *i.e.*,  $J_i^2 = J_{N-i}^2$  and  $b_i = b_{N+1-i}$ , the necessary and sufficient condition for PST is

$$\omega_{k+1} - \omega_k = (2m_k + 1)\pi/t_{\text{PST}}, \quad (4)$$

where the set of eigenenergies  $\{\omega_k\}$  is ordered,  $\omega_k < \omega_{k+1}$ . The condition (4) must be fulfilled for all pairs of successive energies, where the  $m_k$  may be arbitrary integers. The shortest time  $t_{\text{PST}}$  for which (4) is fulfilled is the first time at which PST is achieved [17, 37]. Since (4) implies strictly periodic time evolution, PST occurs again and again, at all odd multiples of  $t_{\text{PST}}$ .

## III. ENERGY AND SPIN-COUPPLING DISTRIBUTIONS

Every set of integers  $m_k$  in (4) leads to a unique energy spectrum enabling PST and hence, as we shall explain below, to a unique set of coupling constants  $J_i$ . Therefore, there are infinitely many spin chains allowing for PST. But, are all of them equally efficient for transferring information? How is their PST capability affected by perturbations through inaccuracies in the coupling constants or from coupling to external degrees of freedom? What properties are necessary to stabilize the system against such perturbations?

We tackle these questions by studying the transmission robustness of different PST channels in the presence of static perturbations. We characterize these spin-channel systems by their energy eigenvalue distributions. A given spectrum that satisfies the condition (4) defines a unique Hamiltonian with positive symmetric couplings  $J_i$ , which can be obtained by solving an inverse eigenvalue problem [38]. For simplicity we choose  $\omega_k = -\omega_{N+1-k}$ ,  $\forall k$ , which imposes  $b_i = 0$ ,  $\forall i$  [37].

In order to study a range of different eigenvalue distributions systematically, we start from the case of an equidistant energy spectrum,  $m_k = \text{const.}$  in (4), which was discussed in Ref. [16]. We vary that spectrum by distributing the energy values more densely either in the center or towards the boundaries of the energy spectrum. The class of energy spectra which we discuss can be parametrized as follows:

$$\omega_k(k_\beta, \alpha) = -A_{(k_\beta, \alpha)} \text{sgn}(k - k_0) [(k_\beta - |k - k_0|)^\alpha - k_\beta^\alpha]. \quad (5)$$

We assume that  $N$  is odd,  $k = 1, \dots, N$  numbers the energy eigenvalues in ascending order, as before, and  $k_0 = \frac{N-1}{2}$  marks the center of the spectrum. The shape of the spectrum is controlled by an exponent  $\alpha$  and a reference index  $k_\beta$  which can assume two values;  $k_\beta = k_b = k_0$  or  $k_\beta = k_c = 0$ . The overall width of the spectrum is controlled by  $A_{(k_\beta, \alpha)}$ . The equidistant energy spectrum (constant density of eigenvalues) is given by  $\omega_k(k_c, 1)$ . The density of eigenvalues in the center of the spectrum increases for both  $\omega_k(k_c, n)$  and  $\omega_k(k_b, \frac{1}{n})$  with integer  $n \geq 2$ . A larger density of eigenvalues close to the boundaries of the spectrum is obtained for  $\omega_k(k_b, n)$  and  $\omega_k(k_c, \frac{1}{n})$ . The shapes of the two spectra defined by these two possibilities for given  $n$  are different, as are those of  $\omega_k(k_c, n)$  and  $\omega_k(k_b, \frac{1}{n})$ , respectively. For non-integer exponent  $\alpha$  the energies (5) normally do not fulfill the commensurability condition (4) and have to be slightly readjusted to make PST possible. Figure 1(a) shows the energy eigenvalues for the equidistant spectrum,  $\omega_k(k_c, 1)$ , along with the four possibilities just discussed, for  $n = 2$ . The corresponding exchange couplings  $J_i$  (normalized by the maximum coupling strength  $J_{max}$ ) are shown in Fig. 1(b). The coupling distribution determines the transmission velocity as we shall discuss in Sec. IV.

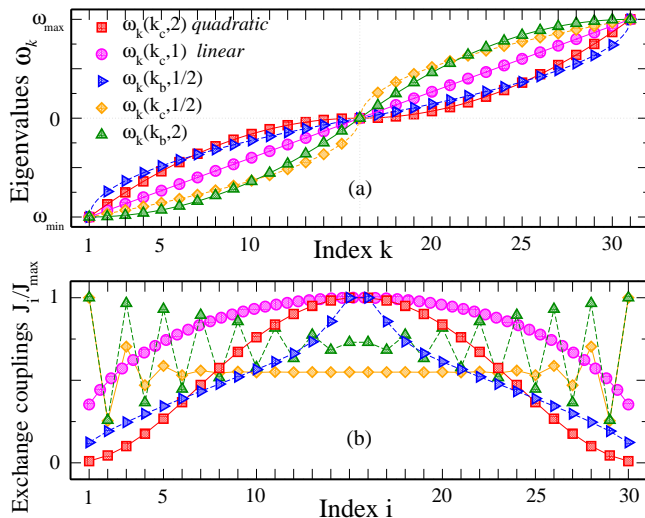


Figure 1: (Color online) (a) Energy eigenvalue distributions  $\omega_k(k_\beta, \alpha)$ . The symbols represent the energy values and the lines give the exact functional dependence of Eq. (5). (b) Exchange couplings determined by solving the inverse eigenvalue problem for each of the spectra given in (a).

#### IV. PERFECT STATE TRANSFER STABILITY OF ENERGY DISTRIBUTIONS

##### A. Unperturbed transfer

To compare the perfect state transfer performance of the spin-channels with the different energy eigenvalue distributions of Fig. 1, we calculated their averaged fidelity (3). Figure 2 shows the fidelity of state transfer from one end of the chain to the other, as a function of time. The time scale is given in units of the first perfect state transfer time  $t_{PST}$ . At this point it is important to note that the dynamics of the system contain at least two other relevant time scales besides the time  $t_{PST}$  which we shall use as a unit of time. The first such time scale is the spin-channel clock time  $2t_M$ , *i.e.*, the characteristic time of the information propagation within the chain, also called mesoscopic echo time [39]. For a chain supporting spin waves as elementary excitations, *e.g.* the uniformly coupled XX or Heisenberg chains,  $t_M$  is fixed by the maximum group velocity of the spin waves [3, 40–42]. The group velocity of excitations with dispersion  $\omega(k)$  (where  $k$  now temporarily denotes the wave number) is given by  $v_g = \frac{d\omega}{dk}$ . Unfortunately this concept breaks down for the systems of interest here, since translational invariance is broken by the non-uniform couplings  $J_i$  and the wave number is no longer defined. Our numerical results show that  $t_{PST}$  can be larger than  $t_M$ , see for example, Fig. 2(c) and (d). At  $t_M$  the excitations created at  $t = 0$  at site  $i = 1$  interfere constructively but not perfectly at site  $i = N$ . Perfect interference occurs only later, at  $t = t_{PST}$ , after the excitations have travelled back and forth between the ends of the chain many more times.

Fig. 2(a) and (b) show that the *linear*  $\omega_k(k_c, 1)$  and *quadratic*  $\omega_k(k_c, 2)$  distributions achieve perfect transfer without secondary maximum of the fidelity at some earlier time. For those two systems  $t_{PST}$  is thus equal to the  $t_M$  of the spin chain. To make a quantitative analysis of the speed of the transfer, we consider as a reference the known value  $t_M^h$  for a homogeneous spin-chain with  $J_i \equiv J$  in Eq. (1). In that system, constructive interference at site  $N$  occurs at time  $t_M^h \sim \frac{N}{2J}$  [42]. The transfer obtained at that instant is not perfect, but by switching couplings on and off to perform consecutive swap operations, perfect transfer may be achieved at  $t_M^{swap} \sim \frac{\pi N}{2J}$  [43]. In terms of the maximum coupling  $J_{max}$ , the PST time for the linear distribution is  $t_{PST}^{linear} = \frac{\pi N}{4J_{max}}$ , which is two times faster than the consecutive swaps assuming  $J = J_{max}$ ,  $t_{PST}^{linear} = \frac{1}{2}t_M^{swap}$ , but slower than the free evolution,  $t_{PST}^{linear} = \frac{\pi}{2}t_M^h$ , in a homogeneous chain. The other distributions are about 15 times slower than the linear case as listed in the caption of 2. The second important time scale is given by the duration of the PST maximum of the fidelity, *i.e.* the time during which the fidelity is very close to unity.  $\Delta t$  can be interpreted as the time of residence of the perfectly transmitted state on the last site of the chain; it determines the timing precision required for perfect state read-out. While the *quadratic* distribution is much slower than the linear one in terms of transfer time, its advantage is a much longer window time. We will return to this point later in Sec. V.

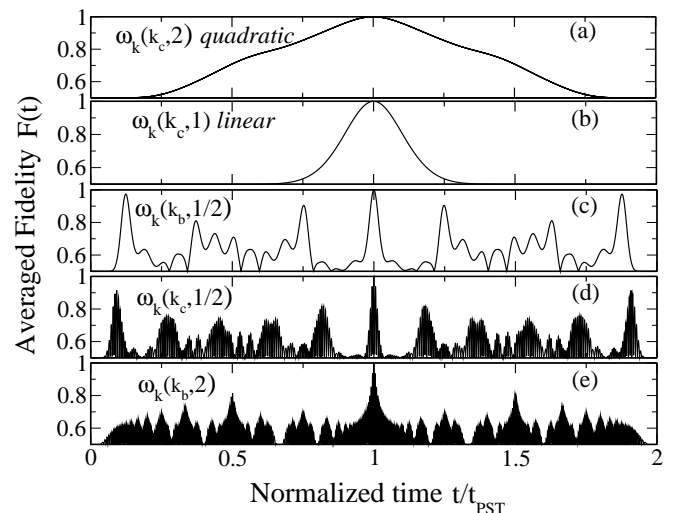


Figure 2: Averaged fidelity of the state transfer in a  $N = 31$  spin chain for the different energy distributions shown in Fig. 1 as a function of time. The *linear*  $\omega_k(k_c, 1)$  and *quadratic*  $\omega_k(k_c, 2)$  distributions achieve the perfect transmission with the first echo, while the other cases achieve it after several echoes. In panels (d) and (e), the black regions are due to fast oscillations because of the coupling strength oscillations shown in Fig. 1b. The transfer times are given by  $t_{PST}^{linear} = \frac{\pi N}{4J_{max}}$  and  $t_{PST} \sim \gamma t_{PST}^{linear}$  with  $\gamma = 15.4, 17, 15, 14.5$  for a *quadratic*,  $\omega_k(k_b, \frac{1}{2})$ ,  $\omega_k(k_c, \frac{1}{2})$  and  $\omega_k(k_b, 2)$  distribution respectively.

## B. Perturbed transfer

So far, we have discussed the performances of different spin-channels without any external perturbation. However, since the perfect engineering of all spin couplings is highly improbable, the study of the performance of different spin-coupling distributions under perturbations by flawed spin couplings becomes relevant. To study the robustness of the spin chains against perturbations we introduce static random spin-coupling imperfections quantified by  $\delta_i$

$$J_i \longrightarrow J_i(1 + \delta_i), \quad (6)$$

where each  $\delta_i$  is an independent uniformly distributed random variable in the interval  $[-\varepsilon_J, \varepsilon_J]$ .  $\varepsilon_J$  is a positive real number that characterizes the maximum perturbation strength relative to  $J_i$ .

We calculate numerically the fidelity time evolution  $\bar{F}(t) = \langle F(t) \rangle_{N_{av}}$  averaged over  $N_{av}$  different realizations of the random imperfection values  $\delta_i$ . Figure 3 shows the averaged fidelity evolution for the different energy eigenvalue distributions for a common  $\varepsilon_J$  value. Only two cases are strongly distinguished by their robustness against the perturbation: the *linear* distribution, which was already studied by De Chiara et. al. [30], and the *quadratic* distribution. As the near-perfect echoes in Fig. 3(a) and (b) show, disorder at the level of  $\varepsilon_J = 10^{-2}$  does not significantly affect PST in those two cases. In contrast, panels (c) and especially (d) and (e) of the same figure show a rather rapid decay of the fidelity (black line) down to a useless level. The colored lines in panels (c), (d) and (e) show the fidelities of the unperturbed systems for comparison.

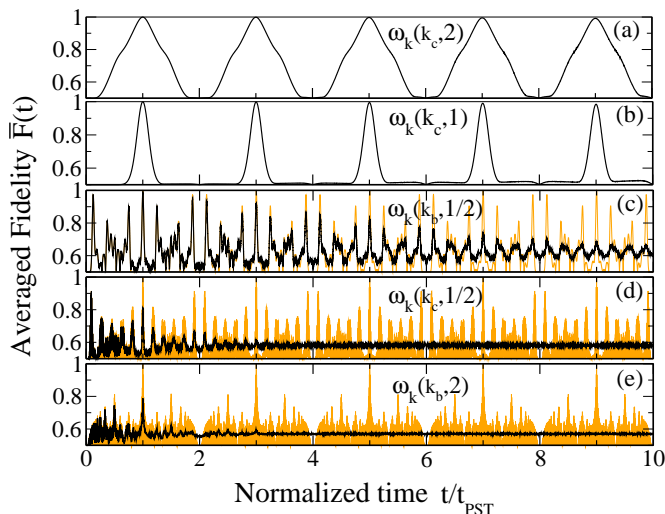


Figure 3: (Color online) Averaged fidelity of the state transfer in a  $N = 31$  spin chain with random perturbations of strength  $\varepsilon_J = 10^{-2}$  averaged over  $N_{av} = 10^2$  realizations for the different energy distributions from Fig. 1 as a function of time. The colored lines in (c), (d) and (e) show  $F(t)$  for the systems without perturbation ( $\varepsilon_J = 0$ ).

Figure 4 shows in detail the comparison of the 9th echo between the *linear* and the *quadratic* distributions. The *quadratic* distribution is obviously more robust than the *linear* distribution, and also its  $\Delta t$  is larger. Also shown are the 9th echoes for  $n = 3$  (colored line) and for  $n = 10$ , respectively. These data show that both the maximum fidelity and the length  $\Delta t$  of the time window for the state read-out increase with  $n$  for energy eigenvalue distributions of type  $\omega_k(k_c, n)$ . However, the increase from  $n = 3$  to  $n = 10$  is insignificant compared to the increase from  $n = 2$  to  $n = 3$ .

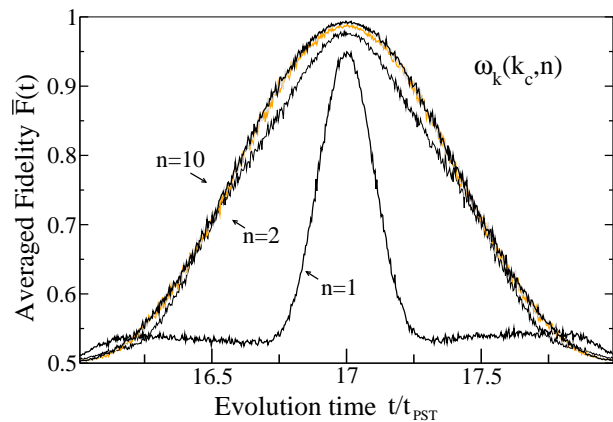


Figure 4: (Color online) Averaged fidelity of the state transfer in a  $N = 31$  spin chain with random perturbations of strength  $\varepsilon_J = 10^{-2}$  averaged over  $N_{av} = 10^2$  realizations for eigenvalue distributions  $\omega_k(k_c, n)$ . Shown is the range of times around the 9th echo of the PST in the unperturbed chain, for  $n = 1, 2, 10$  (black lines), and  $n = 3$  (faint colored line very close to the  $n = 10$  results).

The increase of  $\Delta t$  with growing  $n$  can be explained by the changes of the exchange couplings  $J_i$  shown in Fig. 1(b). When  $n$  changes from 1 to 2 the  $J_i$  decrease close to the boundaries and increase in the center of the chain. This trend continues even more strongly for larger values of  $n$  (data not shown). The small spin couplings close to the boundaries of the chain prevent the spreading of the information once it is localized at one of the chain ends, thus leading to larger values of  $\Delta t$ .

We now focus on  $n = 2$  because the robustness properties are similar for larger values of  $n$ , but it should be kept in mind that energy eigenvalue distributions  $\omega_k(k_c, n)$  with larger  $n$  are generally more robust. To determine the robustness of the different distributions, we calculate the averaged fidelity  $\bar{F}(t_{PST}, \varepsilon_J)$  as a function of the perturbation strength  $\varepsilon_J$  for the first PST time  $t_{PST}$  determined from the unperturbed case. Figure 5 shows results for different energy distributions and for a wide range of perturbation strengths. The *linear* and *quadratic* distributions turn out to be the most robust ones for all perturbation strengths of interest, yielding quite similar results for weak perturbations ( $\varepsilon_J \lesssim 0.2$ ) where the fidelity is larger than  $F = 0.9$ . For larger perturbation strengths, the *quadratic* distribution is most robust.

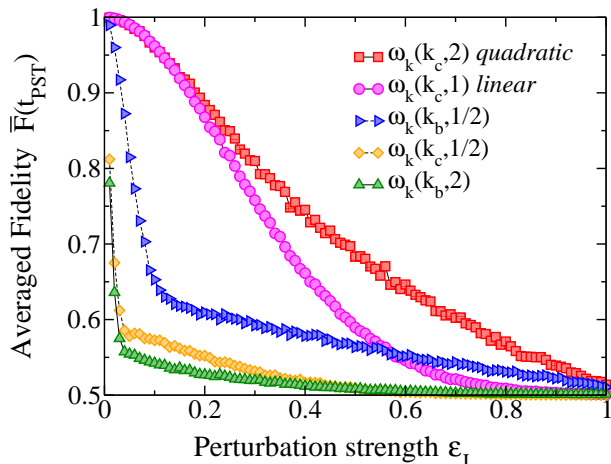


Figure 5: (Color online) Averaged fidelity at time  $t_{PST}$  as a function of the perturbation strength  $\epsilon_J$  for the different energy distributions from Fig. 1 with  $N = 31$  and  $N_{av} = 10^2$ .

Recently, it has been shown that the relative decay of the mesoscopic echoes between a perturbed evolution and the corresponding unperturbed evolution could be used to determine and characterize the decoherence time of the spin-chain channel [44]. Similarly, to determine the decoherence time for each perturbation strength, we study the state transfer fidelity for different PST echoes as a function of their respective PST echo times  $t_{PST}^i = (2i - 1)t_{PST}$ , *i.e.*, the times where the  $i$ -th PST echo arrives at site  $N$  for an unperturbed evolution. Figure 6 shows the fidelity  $\bar{F}(t_{PST}^i, \epsilon_J)$  as a function of  $t_{PST}^i$ , for different perturbation strengths  $\epsilon_J$ . The left panel shows the fidelity for the *quadratic* distribution while the right panel illustrates the *linear* distribution. The decoherence time, *i.e.*, the decay time as a function of  $t_{PST}^i$  is longer for the *quadratic* distribution than for the linear one. Additionally the fidelity of the quadratic distribution converges to an asymptotic value higher than that of the *linear* distribution due to the localization effects caused by the small couplings in the borders, as discussed above. Weak coupling between terminal qubits and the intervening spin chain were used as key elements also in other proposals for quantum information transfer by spin chains recently [11–14, 45].

## V. ROBUSTNESS AND LOCALIZATION

We have shown that certain systems are more robust against perturbations than others. In order to optimize the engineered spin coupling distributions it is decisive to understand which properties of the system are relevant for the robustness of the perfect state transfer. To this end we determine how each energy eigenstate contributes to the dynamics for each of the spin-channels. We expand the states  $|i\rangle$  (a single excitation at site  $i$ ) in the eigenstate basis  $|i\rangle = \sum_k a_{k,i} |\Psi_k\rangle$ , where  $k$  numbers the

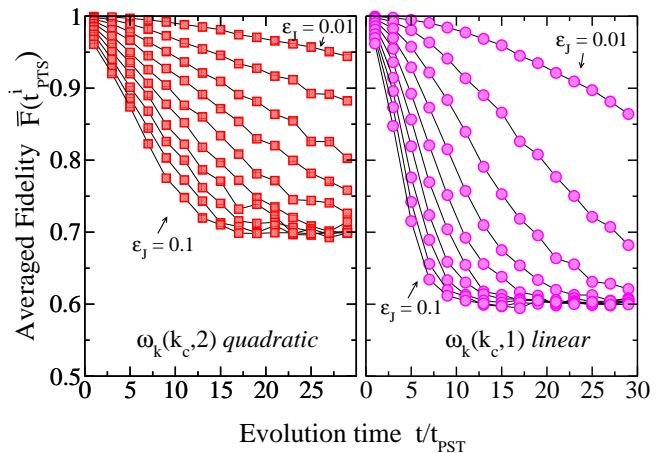


Figure 6: (Color online) Averaged fidelity at odd multiples of  $t_{PST}$  (symbols) for the linear and quadratic energy eigenvalue distributions,  $\omega_k(k_c, n)$  ( $n = 1, 2$ ). Chain length is  $N = 31$ , averages were performed over  $N_{av} = 10^2$  realizations. Perturbation strengths are  $\epsilon = 0.01, 0.02, \dots, 0.1$ .

energy eigenstates in ascending order, as usual. Figure 7 shows the weights  $P_{k,i} = |a_{k,i}|^2$ , for the different energy spectra from Fig. 1. The mirror symmetries with respect to both the center of the chain and the center of the energy spectrum are due to the spatial mirror symmetry of the couplings, and the symmetric tridiagonal nature (with zero diagonal) of the Hamiltonian matrix, respectively. Under perturbations of the couplings the spatial symmetry of the patterns of Fig. 7 is destroyed, while the energetic symmetry is not. We observe that the degree of localization of the energy eigenstates varies strongly between the different eigenvalue distributions. The most robust distributions seem to generate the most strongly localized energy eigenstates; in panels (a), (b) and (c) of Fig. 7 each energy eigenstate basically seems to be localized on two lattice sites. The quadratic distribution [panel (a)] seems to have the most strongly localized eigenstates; in particular the eigenstates that belong to the center of the band are highly localized on the boundaries. This is particularly clear from the upper panels in Fig. 7, showing the contributions  $P_{k,1}$  of the energy eigenstates  $|k\rangle$  to the initial state  $|i = 1\rangle$  with a single excitation localized at the boundary of the chain. In comparison, the other energy distributions show a larger spread in the contributions of the energy eigenstates to each site eigenstate  $|i\rangle$ . Nevertheless, we observe similarities of the distribution of  $P_{k,i}$  between the *linear*, *quadratic* and  $\omega_k(k_b, \frac{1}{2})$  distributions. It has been shown that the presence of localized states at the boundaries of the spin chain can improve the transmission of quantum states [12, 14, 46, 47]. These localized states arise when the coupling of the boundary sites is weaker than the coupling between inner sites or if external fields are applied at the boundary sites. Therefore, we study how the different energy levels are affected by perturbations for the different energy distributions.

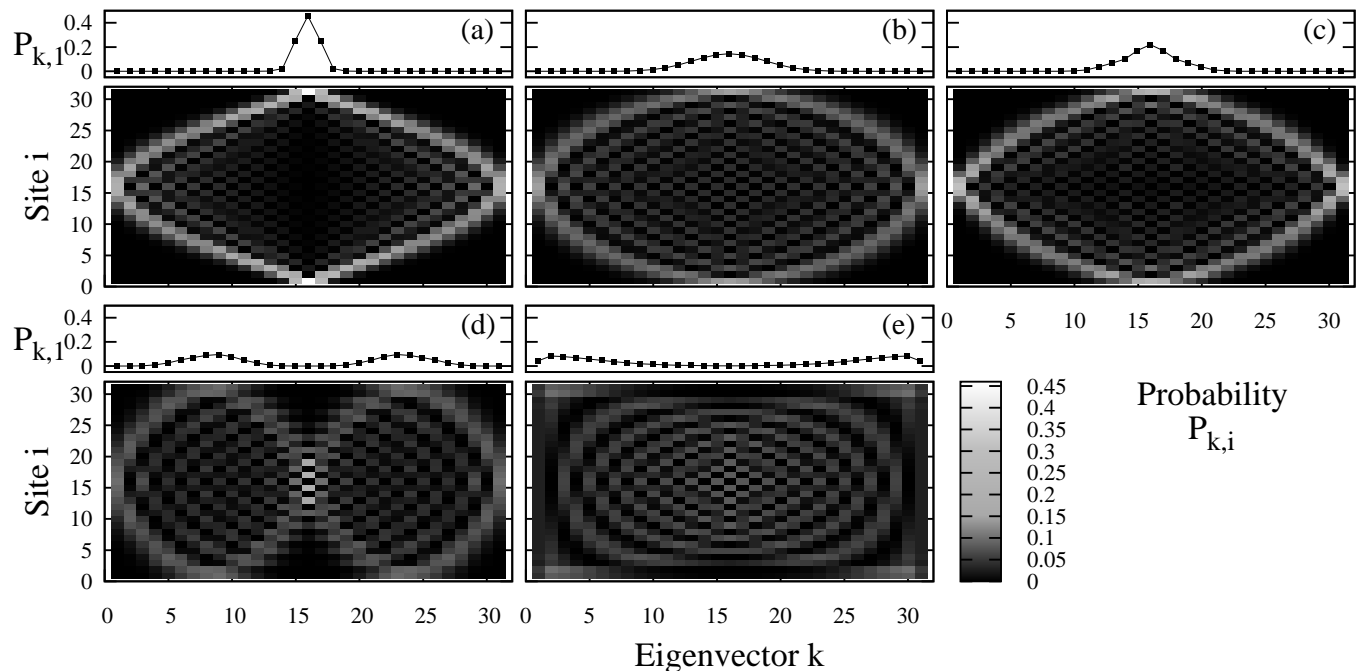


Figure 7: Eigenvector probability  $P_{k,i}$  of the site (computational) states  $|i\rangle$ .  $P_{k,i} = a_{k,i}^2$ , where  $|i\rangle = \sum_k a_{k,i} |\Psi_k\rangle$ . The top part of each panel shows the probabilities  $P_{k,1}$  of the initial state  $|\Psi_0\rangle = |1\rangle$ , and thus shows which energy eigenstates contribute to the state transfer. The panel labels refer to the different energy distributions given in Fig. 1, where a)  $\omega_k(k_c, 2)$  quadratic, b)  $\omega_k(k_c, 1)$  linear c)  $\omega_k(k_b, \frac{1}{2})$ , d)  $\omega_k(k_c, \frac{1}{2})$ , and e)  $\omega_k(k_b, 2)$ .

We generated distributions of energy eigenvalues  $\omega_k$  for the different kinds of unperturbed energy spectra and for different perturbation strengths  $\varepsilon_J$ . For small  $\varepsilon_J$  we observe a symmetric distribution of the perturbed eigenvalues  $\omega_k$  around their respective unperturbed values. The width of that distribution scales with the perturbation strength. For larger values of  $\varepsilon_J$  the distributions of the perturbed  $\omega_k$  become asymmetric with respect to the unperturbed energy level; the low-lying levels tend to be pulled down, while the high-lying levels are pushed up by the same amount. (The energy spectrum of the perturbed Hamiltonian matrix is still symmetric.) The value of  $\varepsilon_J$  where the asymmetry sets in depends on the type of unperturbed energy spectrum and is largest for the quadratic case. To see more quantitatively what is going on in detail, we show in Fig. 8 the standard deviations of the energy levels for the different kinds of unperturbed spectra. Each data point represents an average over  $N_{av} = 10^3$  realizations of the random perturbations. The symmetry of the data with respect to the center  $\omega = 0$  of the energy spectrum and the fact that the zero energy eigenvalue is not affected by the randomness at all are due to the nature (symmetric, tridiagonal, zero diagonal elements) of the Hamiltonian matrix. The key observation explaining the differences in state transfer robustness is made by combining figures 8 and the upper panels of Fig. 7. Those panels show that for the quadratic energy spectrum  $\omega_k(k_c, 2)$  the initial state ( $i = 1$ ) of the state transfer process is superposed from a

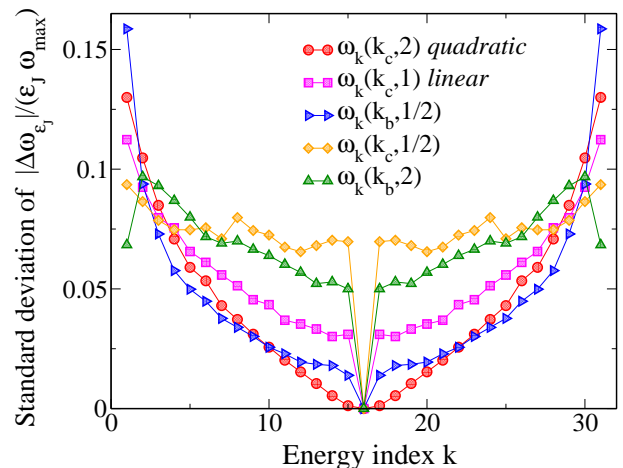


Figure 8: (Color online) Standard deviation of the energy levels  $|\Delta\omega_{\varepsilon_J}| = |\omega_{\varepsilon_J} - \omega_0|$  due to the perturbation with strength  $\varepsilon_J$  for the different energy distributions of Fig. 1. For weak perturbations (small  $\varepsilon_J$ ) the standard deviation turns out to be proportional to  $\varepsilon_J \omega_{max}$ , which we use as a unit here. The data shown are for  $\varepsilon_J < 0.1$ ;  $N_{av} = 10^3$  realizations were used for the calculations.

small number of energy eigenstates in the center of the energy spectrum. In all other types of energy spectrum the initial state shows a wider distribution in the energy quantum number  $k$ . At the same time, the sensitivity to perturbations (which is what is shown in Fig. 8) shows

a comparatively wide minimum with value zero in the center of the spectrum, whereas all other types of spectra show roughly constant nonzero values in the central region of the spectrum, with a single exceptional zero right in the center. The observed particular robustness of the *quadratic* energy spectrum can thus be ascribed to the fact that the initial state consists of a particularly small number of energy eigenstates coming from a part of the energy spectrum which is particularly insensitive to perturbations in the spin coupling constants. For the less robust distributions, the variance is roughly independent of the energy in the center of the energy band, while for the quadratic energy spectrum the variance decreases continuously towards the band center. For that distribution (and for the two other distributions shown in the upper panels of Fig. 7) all energy eigenstates are quite strongly localized. A glance at Fig. 1b shows that the corresponding coupling patterns have the smallest couplings close to the ends of the chain, in the region where those energy eigenstates are localized which are most important for the state transfer. Since we discuss a constant *relative* strength  $\varepsilon$  of the disorder, the *absolute* changes of the couplings tend to be smallest near the ends of the chain, causing only small changes in the energy eigenvalues. That explains the particular robustness of the quadratic distribution.

Another important aspect characterizing the robustness of the transmission is the length of the window of time where high fidelity is obtained for the transmitted state. In this context, we are not only considering errors in the engineered spin couplings, but also the timing error of the measurement [18]. To that end we analyze the term  $|f_N(t)|^2 = |\langle \mathbf{N} | e^{-iHt/\hbar} | \mathbf{1} \rangle|^2$  from (3) at time  $t_{PST} + \delta t$ . Taking into account the spatial symmetry,  $|f_N(t_{PST} + \delta t)|^2$  is given by

$$\begin{aligned} |f_N|^2 &= \left| \sum_{k,s} (-1)^{k+s} P_{s,1} P_{k,1} e^{-i(\omega_k - \omega_s)(t_{PST} + \delta t)} \right| \\ &\approx \left| \sum_{k,s} P_{s,1} P_{k,1} (1 - \delta t(\omega_k - \omega_s) + \right. \\ &\quad \left. i^2 \frac{\delta t^2}{2!} (\omega_k - \omega_s)^2 - \dots) \right| \\ &\approx 1 - \frac{\delta t^2}{2!} \sum_{k,s} P_{s,1} P_{k,1} (\omega_k - \omega_s)^2, \end{aligned} \quad (7)$$

where  $P_{k,i} = |\langle \Psi_k | \mathbf{1} \rangle|^2$ . Even without the Bloch-sphere average (3) which would be necessary for a comparison with Fig. 2, the above result shows why the quadratic distribution displays the longest window of time. The probabilities  $P_{k,1}$  (see Fig. 7) are sharply peaked in the center of the energy band and essentially zero otherwise. Furthermore, due to the quadratic nature of the energy

spectrum, the relevant energy differences  $\omega_k - \omega_s$  are particularly small (see Fig. 1a) making the fidelity deviate from unity only at rather large  $\delta t$  values.

## VI. CONCLUSION

We have studied the robustness of spin chain systems designed for perfect quantum state transfer (PST) under static perturbations. We explored different PST systems by choosing different energy spectra distributions that satisfy the PST conditions. From the energy spectrum of a given chain, the spin-spin coupling constant pattern can be obtained by solving an inverse eigenvalue problem. The robustness of each system was studied by calculating its transmission fidelity under static perturbations of the couplings. We found that robustness is characterized by two main features. One is the reduction of the transfer fidelity induced by the perturbed couplings and the other is the duration of the time window during which the transmitted state may be read out with high fidelity. The most robust systems are those with linear and quadratic energy eigenvalue distributions. These systems achieve PST at the time of the first fidelity maximum. That time may be called the spin-wave echo time, and the less robust systems reach PST only after several spin-wave echoes. By analyzing how the energy eigenstates and eigenvalues are affected by the perturbations, we found that the most robust distributions have strongly spatially localized eigenstates. Thus, because the initial state is localized in one end of the chain, only few eigenstates participate in the transfer. Because of the localization properties of the eigenstates the perturbations in the spin couplings close to the chain boundaries are the only significant source of errors. Since these couplings are rather weak for the most robust systems, a given relative perturbation strength only causes a small absolute perturbation in the couplings and thus in the energy eigenvalues, leading to the observed robustness. The weak couplings close to the ends of the chain also lead to a longer residence time of the transmitted state at its target site at the chain boundary, causing a longer time window for read-out.

## Acknowledgments

We acknowledge support from SECYT-UNC (Universidad Nacional de Córdoba, Argentina), and CONICET (Argentina) for partial financial support of this project. A. Z. thanks CONICET and DAAD, and G. A. A. the Alexander von Humboldt Foundation, for their Research Scientist Fellowships, and the hospitality of Fakultät Physik of TU Dortmund. We also thank P. Karbach for helpful discussions and for his inverse eigenvalue program.

[1] T. D. Ladd, F. Jelezko, R. Laflamme, Y. Nakamura, C. Monroe and J. L. O'Brien, *Nature* **464**, 45 (2010).

[2] D. P. DiVincenzo, *Science* **270**, 255 (1995).

- [3] S. Bose, Phys. Rev. Lett. **91**, 207901 (2003).
- [4] V. Subrahmanyam, Phys. Rev. A **69**, 034304 (2004).
- [5] T. J. Osborne and N. Linden, Phys. Rev. A **69**, 052315 (2004).
- [6] T. Shi, Y. Li, Z. Song and C.-P. Sun, Phys. Rev. A **71**, 032309 (2005).
- [7] J. Fitzsimons and J. Twamley, Phys. Rev. Lett. **97**, 090502 (2006).
- [8] L. Campos Venuti, C. Degli Esposti Boschi and M. Roncaglia, Phys. Rev. Lett. **99**, 060401 (2007).
- [9] F. Plastina and T. J. G. Apollaro, Phys. Rev. Lett. **99**, 177210 (2007).
- [10] C. Di Franco, M. Paternostro and M. S. Kim, Phys. Rev. Lett. **101**, 230502 (2008).
- [11] A. Wójcik, T. Łuczak, P. Kurzyński, A. Grudka, T. Gdala, and M. Bednarska, Phys. Rev. A **72**, 034303 (2005).
- [12] A. Zwick and O. Osenda, J. Phys. A: Math. Theor. **44**, 105302 (2011).
- [13] L. Bianchi, T. J. G. Apollaro, A. Cuccoli, R. Vaia, and P. Verrucchi, Phys. Rev. A **82**, 052321 (2010).
- [14] N. Y. Yao, L. Jiang, A. V. Gorshkov, Z.-X. Gong, A. Zhai, L.-M. Duan, and M. D. Lukin, Phys. Rev. Lett. **106**, 040505 (2011).
- [15] C. Albanese, M. Christandl, N. Datta and A. Ekert, Phys. Rev. Lett. **93**, 230502 (2004).
- [16] M. Christandl, N. Datta, A. Ekert and A. J. Landahl, Phys. Rev. Lett. **92**, 187902 (2004).
- [17] P. Karbach and J. Stolze, Phys. Rev. A **72**, 030301(R) (2005).
- [18] A. Kay, Phys. Rev. A **73**, 032306 (2006).
- [19] Z. L. Mádi et al., Chem. Phys. Lett. **268**, 300 (1997).
- [20] M. A. Nielsen, E. Knill and R. Laflamme, Nature **396**, 6706 (1998).
- [21] J. Zhang, G. L. Long, W. Zhang, Z. Deng, W. Liu and Z. Lu, Phys. Rev. A **72**, 012331 (2005).
- [22] J. Zhang, N. Rajendran, X. Peng and D. Suter, Phys. Rev. A **76**, 012317 (2007).
- [23] G. A. Álvarez, M. Mishkovsky, E. P. Danieli, P. R. Levstein, H. M. Pastawski and L. Frydman, Phys. Rev. A **81**, 060302(R) (2010).
- [24] P. Cappelaro, C. Ramanathan and D. G. Cory, Phys. Rev. A **76**, 032317 (2007).
- [25] E. Rufeil-Fiori, C. M. Sánchez, F. Y. Oliva, H. M. Pastawski, and P. R. Levstein, Phys. Rev. A **79**, 032324 (2009).
- [26] P. Neumann et al., Nat. Phys. **6**, 249 (2010).
- [27] P. Cappelaro, L. Jiang, J. S. Hodges, and M. D. Lukin, Phys. Rev. Lett. **102**, 210502 (2009).
- [28] N. Y. Yao, L. Jiang, A. V. Gorshkov, P. C. Maurer, G. Giedke, J. I. Cirac, and M. D. Lukin, e-print arXiv:1012.2864 [quant-ph].
- [29] W. H. Zurek, Rev. Mod. Phys. **75**, 715 (2003).
- [30] G. De Chiara, D. Rossini, S. Montangero and R. Fazio, Phys. Rev. A **72**, 012323 (2005).
- [31] J. P. Keating, N. Linden, J. C. F. Matthews, and A. Winter, Phys. Rev. A **76**, 012315 (2007).
- [32] C. K. Burrell and T. J. Osborne, Phys. Rev. Lett. **99**, 167201 (2007).
- [33] J. Allcock and N. Linden, Phys. Rev. Lett. **102**, 110501 (2009).
- [34] G. A. Álvarez and D. Suter, Phys. Rev. Lett. **104**, 230403 (2010).
- [35] R. Ronke, T. P. Spiller and I. D'Amico, Phys. Rev. A **83**, 012325 (2011).
- [36] M.-H. Yung, Phys. Rev. A **74**, 030303 (R) (2006).
- [37] A. Kay, Int. J. Quantum Inf. **8**, 641 (2010).
- [38] G. M. L. Gladwell, Inverse Problems in Vibration, Kluwer Academic, Boston (1986).
- [39] V. N. Prigodin, B. L. Altshuler, K. B. Efetov, and S. Iida, Phys. Rev. Lett. **72**, 546 (1994).
- [40] H. M. Pastawski, P. R. Levstein, and G. Usaj, Phys. Rev. Lett. **75**, 4310 (1995).
- [41] H. M. Pastawski, G. Usaj, and P. R. Levstein, Chem. Phys. Lett. **261**, 329 (1996).
- [42] E. B. Fel'dman, R. Bruschweiler and R. R. Ernst, Chem. Phys. Lett. **294**, 297 (1998).
- [43] D. Petrosyan, G. M. Nikolopoulos and P. Lambropoulos, Phys. Rev. A **81**, 042307 (2010).
- [44] G. A. Álvarez, E. P. Danieli, P. R. Levstein, H. M. Pastawski, Phys. Rev. A **82**, 012310 (2010).
- [45] S. Oh, L.-A. Wu, Y.-P. Shim, M. Friesen, X. Hu, Arxiv 1102.0762 (quant-ph).
- [46] G. Gualdi, V. Kostak, I. Marzoli, and P. Tombesi, Phys. Rev. A **78**, 022325 (2008).
- [47] T. Linneweber, J. Stolze and G. S. Uhrig, to be published.